Biophysical and Structural Characterization of Ribulose-5-phosphate Epimerase from *Leishmania donovani*

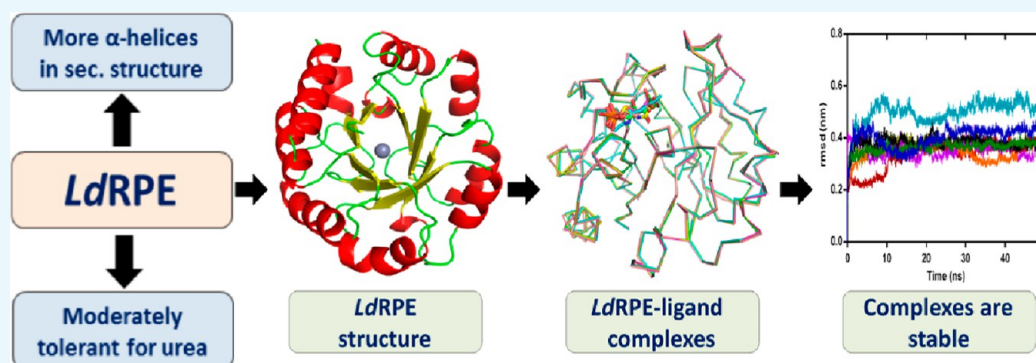Bandigi Narsimulu, Rahila Qureshi, Pranay Jakkula, Sayanna Are, and Insaf Ahmed Qureshi*

ACCESS | Metrics & More | Article Recommendations

ABSTRACT: Pentose phosphate pathway (PPP) plays a crucial role in the maintenance of NADPH/NADP$^+$ homeostasis and provides protection against oxidative stress through detoxification of the reactive oxygen species. Ribulose-5-phosphate epimerase (RPE) participates in catalysis of the interconversion of ribulose-5-phosphate (Ru5P) to xylulose-5-phosphate (Xu5P) during PPP, however the structural attributes of this enzyme are still underexplored in many human pathogens including leishmanial parasites. The present study focuses upon cloning, purification and characterization of RPE of *Leishmania donovani* (*Ld*RPE) using various biophysical and structural approaches. Sequence analysis has shown the presence of trypanosomatid-specific insertions at the N-terminus that are absent in humans and other eukaryotes. Gel filtration chromatography indicated recombinant *Ld*RPE to exist as a dimer in the solution. Circular dichroism studies revealed a higher alpha helical content at physiological pH and temperature that comparatively varies with changing these parameters. Additionally, intrinsic fluorescence and quenching studies of *Ld*RPE have depicted that tryptophan residues are mainly buried in the hydrophobic regions, and the recombinant enzyme is moderately tolerant to urea. Moreover, homology modeling was employed to generate the three-dimensional structure of *Ld*RPE followed by molecular docking with the substrate, product, and substrate analogues. The modeled structure of *Ld*RPE unravelled the presence of conserved active site residues as well as a single binding pocket for the substrate and product, while an *in silico* study suggested binding of substrate analogues into a similar pocket with more affinity than the substrate. Additionally, molecular dynamics simulation analysis has deciphered complexes of *Ld*RPE with most of the ligands exhibiting more stability than its apo form and lesser fluctuations in active site residues in the presence of ligands. Altogether, our study presents structural insights into leishmanial RPE that could provide the basis for its implication to develop potent antileishmanials.

1. INTRODUCTION

Trypanosomatid protozoan parasite *Leishmania* is responsible for the disease leishmaniasis, which affect millions of people worldwide. The parasite causes a spectrum of diseases ranging from simple, self-healing innocuous oriental shore to fatal visceral leishmaniasis. It is transmitted to the mammalian hosts through the bite of sandfly belonging to the genus Phlebotomus.[1] The amastigote and promastigote stages of the parasite survive and propagate inside the parasitophorous vacuole of the host macrophage and midgut of the sandfly, respectively.[2,3] The infected macrophage provides a first-line antimicrobial defence through the production of reactive oxygen species (ROS) and creating the oxidative stress that is

harmful for the survival of parasites. To overcome this problem in the parasite most of the glucose molecules undergo in pentose phosphate pathway (PPP) to produce NADPH that reduces the oxidative stress environment surrounding the parasite and makes the PPP a vital part of the defence
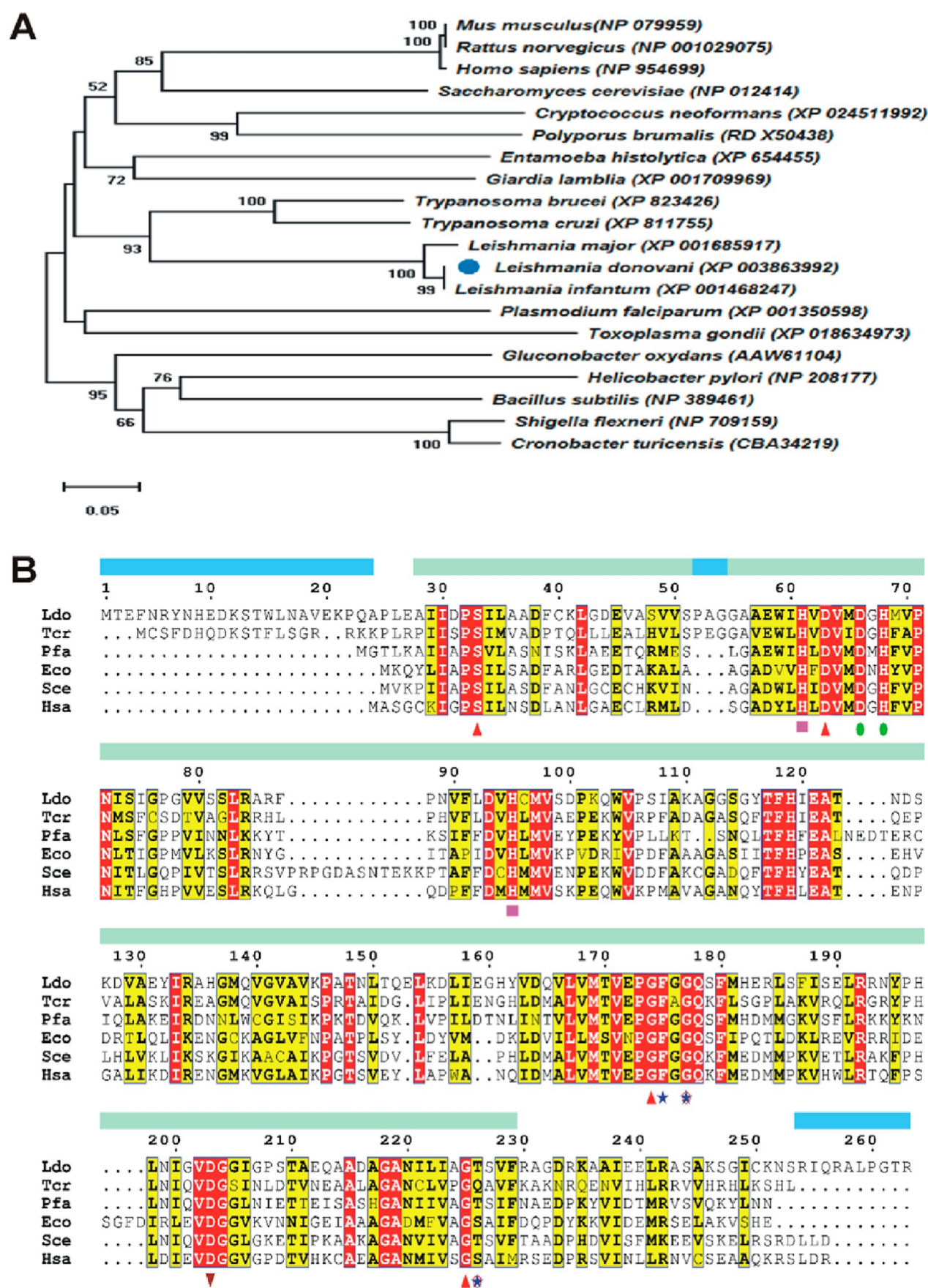
Figure 1. Phylogenetic and sequence analysis of *Ld*RPE. (A) Phylogenetic tree was generated using RPE protein sequences from various organisms through the neighbor-joining method. The numbers before the branch points delineate the confidence level of the relationship of the paired sequences determined by 1000 bootstrap statistical analysis. (B) Multiple sequence alignment of *Ld*RPE was carried out with its counterpart from

Figure 1. continued

T. cruzi (Tcr), *P. falciparum* (Pfa), *H. sapiens* (Hsa), *E. coli* (Eco), and *S. cerevisiae* (Sce). The sequence is numbered according to *Ld*RPE with conserved and similar residues highlighted as red and yellow, respectively. The RPE domain is presented as a box with green color, wherein insertions of amino acids are shown as blue boxes. Blue stars and red triangles indicate the substrate and product binding residues, respectively, with circled stars representing the residues binding with both the substrate and product. Green circles display the residues involved in dimeric interface formation, while pink square boxes denote the metal binding residues and red inverted triangles delineate the residue interacting with the substrate, product, and metal.

mechanism.[4,5] The PPP initiates with glucose-6-phosphate, the primary intermediate of the metabolic route. This pathway contains two branches, the oxidative branch that produces ribulose-5-phosphate (Ru5P) from glucose 6-phosphate by reducing two $NADP^+$ molecules and the non-oxidative stage that eventually functions in succession, leading back to the intermediates of glycolysis.

The PPP typically functions in two important pathways, namely, the generation of NADPH from $NADP^+$ and production of ribose-5-phosphate (R5P). NADPH is an indispensable coenzyme for biosynthetic reactions along with providing protection to cells to counter the oxidative stress executed by ROS, whereas R5P plays a significant role in the production of DNA, RNA, and erythrose-4-phosphate (E4P), a precursor of vitamin B6 and aromatic amino acids.[5] Ribulose-5-phosphate epimerase (RPE) is an enzyme of the non-oxidative branch of the PPP and is responsible for reversible conversion of Ru5P to xylulose-5-phosphate (Xu5P). RPEs are widely present in three important kingdoms, namely, bacteria, fungi, and most of the eukaryotic organisms.[6−10] Studies in many organisms have shown this enzyme to utilize the divalent cations as activators or cofactors and had largely regarded it as a metalloenzyme.[8,11,12] RPE has been considered as a primary target of oxidative stress in *Escherichia coli* produced by hydrogen peroxide;[13] moreover, the absence of functional RPE in the yeast was associated with its susceptibility to oxidative stress.[14] RPE also acts as a precursor in the shikimate pathway, a vital pathway in *Plasmodium falciparum,* and its deficiency has negatively affected the primary substrate (E4P) of this pathway.[11]

The PPP is restricted to the cytosol of most of the organisms, but it is localized between glycosomes and cytosol in trypanosomatids.[15] Further, complete genome sequencing of several trypanosomatids including *Leishmania* and *Trypanosoma* parasites has added extensive knowledge regarding these enzymes. Based on the presence and absence of a peroxisomal targeting signal, two isoenzymes are known to be encoded by *Leishmania* as well as *Trypanosoma cruzi*,[10,16] and the first enzyme was found in promastigotes of *Leishmania mexicana* with a threefold higher occurrence than its competitor enzyme (RPI-B, ribose-5-phosphate isomerase type B).[17] Although the two isoenzymes of *T. cruzi* are highly similar at the sequence level, cytosolic *Tc*RPE1 displays a higher specific activity as compared to its isoenzyme, glycosomal *Tc*RPE2.[10] Moreover, genome-wide RNAi studies in *Trypanosoma brucei* employing RIT-seq indicated that depleted mRNA had not resulted in hampered fitness, and its activity was not identified in parasites isolated from the mice, inferring that RPE might not be categorized as a drug target in *T. brucei*.[18−20] However, no significant study is available in other trypanosomatid parasites including *Leishmania*.

Enzymes of the oxidative branch of the PPP have been reported in many protozoan parasites including *Plasmodium*, *Trypanosoma*, and so forth,[20−23] but very limited biochemical and structural information is available for a majority of the enzymes belonging to the non-oxidative branch such as RPE. Our study presents the first report of molecular cloning and purification of RPE from the leishmanial parasite succeeded by biophysical and structural characterization. Simultaneously, analogues of R5P were analyzed through an *in silico* approach to identify the potential lead compounds against leishmanial parasites.

2. RESULTS

2.1. Sequence and Phylogenetic Analysis of *Ld*RPE. The protein sequence of *Leishmania donovani* RPE (*Ld*RPE), comprising 263 amino acids, revealed neither transmembrane domain nor signal peptides, while the calculated molecular weight was found to be 28,275.05 Da. It had shown the isoelectric point and instability index as 5.71 and 44.47, respectively, delineating more negative charged residues and its slightly unstable nature. The grand average of hydropathicity was enumerated as −0.122, suggesting the *Ld*RPE to be moderately hydrophobic. *Ld*RPE possessed a single domain (29−229 amino acids) containing catalytic residues that interact with the substrate (Ru5P), product (Xu5P), and cofactor (divalent metal ion). To enrich our understanding regarding the evolutionary relationship among the known RPE proteins, a phylogenetic tree was constructed employing protein sequences from 20 organisms. The phylogenetic analysis showed that *Ld*RPE is closely related to protozoan parasites such as *L. major*, *L. infantum*, *T. cruzi*, *T. brucei*, *Entamoeba histolytica*, and *Giardia lamblia* that are present in neighboring clusters, while bacterial RPE protein sequences were observed to be located in different groups of the phylogenetic tree. Apicomplexan parasites such as *Toxoplasma* and *Plasmodium* were found to be in a separate clade and exhibited less divergence from *Ld*RPE, whereas RPEs of different clusters encompassing organisms such as *Homo sapiens*, *Rattus norvegicus*, and *Mus musculus* are highly divergent from the leishmanial RPE (Figure 1A).

In order to identify the catalytic residues of leishmanial RPE, multiple sequence alignment was carried out and it reflected two trypanosomatid-specific insertions (1−23 and 52−54) at the N-terminus and another stretch of 11 residues (253−263) at the C-terminus in *Ld*RPE. Furthermore, residues of the catalytic domain were predominantly conserved for ligand binding in RPEs of *L. donovani*, *T. cruzi*, *P. falciparum*, and *H. sapiens* (Figure 1B). The substrate (Ru5P) binding site was marked by the residues Gly177, Gly205, Asp203, Gly225, and Thr226, while Asp63, Gly177, Gln178, Asp203, Gly205, Gly225, and Thr226 form the binding site for the product (Xu5P). Remarkably, Thr226 of *Ld*RPE is replaced by Ser201 in its human counterpart with remaining catalytic residues to be conserved.
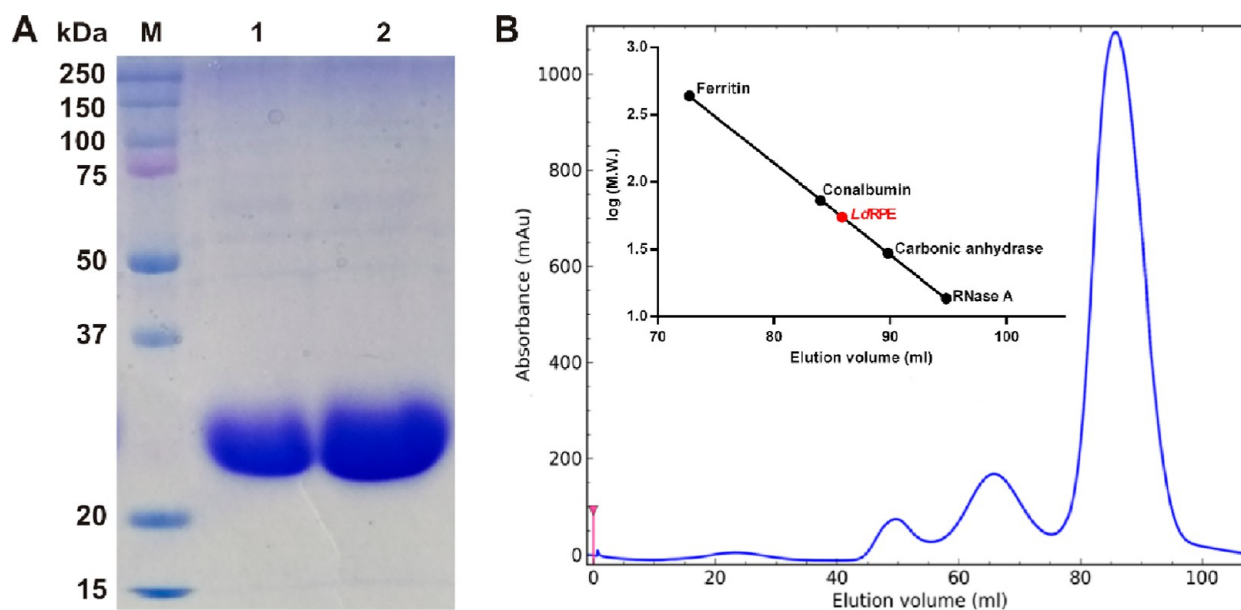
Figure 2. Purification and molecular weight determination of recombinant *Ld*RPE. (A) 10% SDS-PAGE of purified *Ld*RPE. Lane M shows the pre-stained protein marker, while lanes 1 and 2 indicate purified fractions. (B) Size exclusion chromatography profile of *Ld*RPE displaying elution at 85.7 mL on a Superdex 16/600 200 pg corresponding to a molecular weight of 62.4 kDa. The inset demonstrates the resultant plot of protein standards such as ferritin (440 kDa), conalbumin (75 kDa), carbonic anhydrase (29.0 kDa), and RNase A (13.7 kDa) along with *Ld*RPE (red circle) in buffer comprising 20 mM 4-(2-hydroxyethyl)-1-piperazineethanesulfonic acid (HEPES) pH 7.5 and 100 mM KCl.
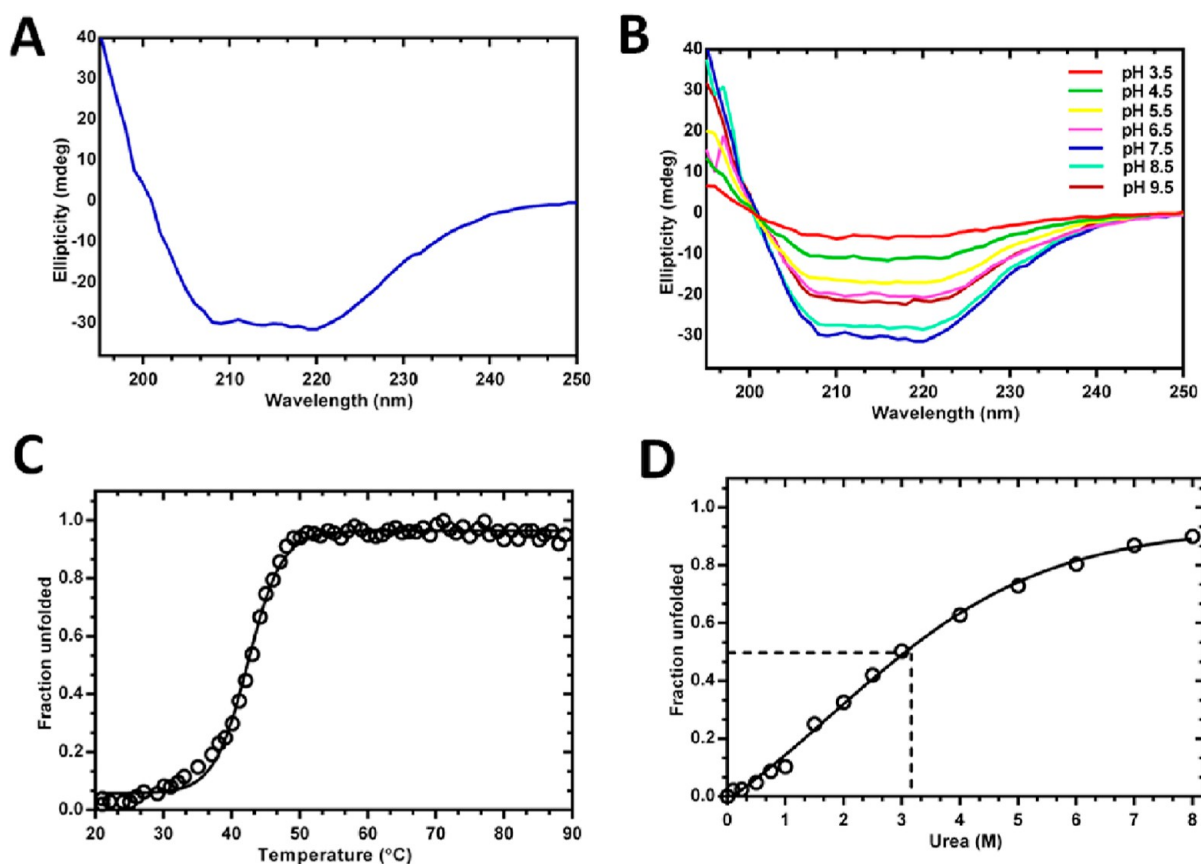
Figure 3. Effect of pH, temperature, and urea on the secondary structure of *Ld*RPE. Far UV-CD spectra were taken from 250 to 195 nm using 5 μM of protein at pH 7.5 (A) and different pH (B). Normalized thermal denaturation plot with temperature from 20 to 90 °C (C). Far-UV CD spectra at 222 nm with various concentrations of urea were plotted and fit into a two-state equation (D).

2.2. Cloning and Purification of *Ld*RPE. The full-length open reading frame (ORF) of *Ld*RPE was cloned into expression vector pET28a(+), and the resultant construct was transformed into *E. coli* BL21(DE3) cells. The

Table 1. Secondary Structural Contents of *Ld*RPE with Varying pH

Secondary structure	pH 3.5	pH 4.5	pH 5.5	pH 6.5	pH 7.5	pH 8.5	pH 9.5
α-helix	23	30	29	28	37	33	28
β-sheet	25	17	20	17	18	17	23
Random coil	52	53	51	55	45	50	49

recombinant protein with an N-terminal His-tag was expressed in bacterial cells followed by purification from the soluble fraction of the cell lysate through affinity chromatography. The quality of protein was assessed on 10% sodium dodecyl sulphate-polyacrylamide gel electrophoresis (SDS-PAGE) showing a single band at a molecular weight of approximately 31 kDa, which was similar to its predicted molecular weight (Figure 2A). Subsequently, size-exclusion chromatography was employed to analyze the oligomeric state of *Ld*RPE in solution. The protein was eluted as three peaks, with the first and second small peaks indicating higher oligomeric forms and a third large and predominant peak corresponding to the value close to 62.4 kDa, suggesting the dimeric state of *Ld*RPE in the solution (Figure 2B).

2.3. Secondary Structure Analysis of *Ld*RPE. Far-UV circular dichroism (CD) spectroscopy was employed to analyze the secondary structural features of the purified *Ld*RPE. CD spectra of *Ld*RPE depicted a negative peak at 222 and 208 nm, indicating the alpha helix as a dominant secondary structure. Subsequently, the DichroWeb server was used to predict the secondary structure elements of the protein that unravel 37% of α-helices, 18% of β-strands, and 45% of random coils at pH 7.5 (Figure 3A). Further, folding of leishmanial protein was analyzed with varying pH, and structural conformation was found to be adequate at pH 7.5. However, there was a reduction in the ellipticity at acidic and basic pH, which advocated toward loss of the secondary structure (Figure 3B, Table 1).

To understand the effect of temperature on *Ld*RPE, a thermal denaturation study was performed that exhibited cooperative unfolding with an increase in the temperature, and the computed T_m was found to be 43 °C (Figure 3C). Subsequently, the effect of 0 to 8 M urea was assessed on the secondary structure of the recombinant protein that delineated only 20% loss of the secondary structure up to 2 M urea, whereas further increase in urea concentration from 2 to 6 M resulted in approximately 80% ellipticity loss. The complete loss of the secondary structure was observed at 7 and 8 M urea concentrations, and the mid-transition concentration of urea (C_m) was calculated to be 3.1 M (Figure 3D), which indicates that *Ld*RPE has moderate tolerance to urea.

2.4. Intrinsic Fluorescence Measurements of *Ld*RPE. The intrinsic fluorescence of a protein mainly depends on the tryptophan (Trp) and tyrosine (Tyr) fluorophores, which are very sensitive to the microenvironment. The *Ld*RPE protein possesses three Trp residues at 15, 59, and 104 and five Tyr residues at 7, 116, 132, 162, and 195 positions. At pH 7.5, *Ld*RPE has shown a maximum emission wavelength at 340 nm that indicates partial exposure of the Trp residue to the solvent environment (Figure 4A). The conformational changes of *Ld*RPE were monitored at different pH through the changes in the fluorescence spectra, which displayed a gradual increase in intensity with a decrease in pH from 7.5 to 3.5 without a change in the maximum emission that delineates minor structural changes in the tryptophan microenvironment. Notably, the fluorescence emission wavelength has a red shift

from 340 nm (pH 7.5) to 343 nm at pH 8.5 and 9.5 (Figure 4B). This illustrates the higher accessibility of the tryptophan residues to the solvent environment when pH was changed from neutral to basic conditions. Furthermore, an extrinsic fluorescent dye[(8-anilino-1-naphthalenesulfonic acid (ANS)] was used for monitoring the structural changes upon unfolding of *Ld*RPE at different pH (3.5 to 9.5). ANS binding studies revealed that the λ_{max} was 490 nm at pH 7.5 (Figure 4C), suggesting that the protein retains its native form. Further, the fluorescence intensity was decreased with no change in the maximum wavelength at pH 8.5 and 9.5, displaying similar conformation of the protein. However, there was an approximately threefold increase in fluorescence intensity, and the emission maximum shifted from 490 to 475 nm (15 nm blue shift) at pH 3.5 to 6.5, which delineates the aggregation of the protein (Figure 4D). In addition, tryptophan fluorescence emission spectra were also used to study the thermal denaturation of apo *Ld*RPE and its complex with Ru5P. The peak of maximum fluorescence intensity was observed at 340 nm, whereas further increase in temperature at every 5 °C interval resulted in a gradual decrease of fluorescence intensities (Figure 4E,G). Moreover, the intensity had dropped by about 4.4 and 8.3 times at 90 °C in comparison to that at 20 °C for apo and complex *Ld*RPE, respectively. The fraction that unfolded as a function of temperature depicted a sigmoidal curve that was fitted into a two-state equation, and T_m for apo and complex *Ld*RPE were calculated to be 43 and 55 °C, respectively (Figure 4F,H). It indicates that the presence of a substrate with a protein had increased the structural integrity due to which it started to unfold at a higher temperature as compared to the apo form.

Furthermore, a fluorescence study was employed to evaluate the binding affinity of *Ld*RPE with divalent metal ions. The fluorescence emission maximum of *Ld*RPE was found to gradually decrease with increasing concentrations of divalent ions (Mn^{2+}, Zn^{2+}, Fe^{2+}, and Mg^{2+}), which suggests interaction of these metals with the protein (Figure 5).

The binding constants (K_a) were determined by the modified Stern−Volmer plots, which demonstrated that manganese has the highest binding affinity with a K_a value of 246 ± 7.1 M^{-1}, while magnesium displayed the lowest binding affinity of 22.6 ± 1.3 M^{-1} among the tested metal ions (Figure 5, Table 2). The binding affinity of manganese was approximately 1.6, 3.0, and 10.8 times higher in comparison to that of zinc, iron, and magnesium, respectively.

2.5. Evaluation of Tryptophan Positions in *Ld*RPE. Computational prediction with the WESA server revealed that *Ld*RPE sequence encompasses three tryptophan residues, wherein one (Trp15) is present on the surface of the protein and two (Trp59 and Trp104) are buried. Fluorescence quenching studies were performed with the increasing concentration of acrylamide and potassium iodide (KI). The fluorescence intensity steadily decreased with increasing concentrations of quenchers with a reduction by 2.0 and 1.7 times in the presence of 1 M acrylamide and KI, respectively (Figure 6A,C). It advocates that acrylamide being neutrally
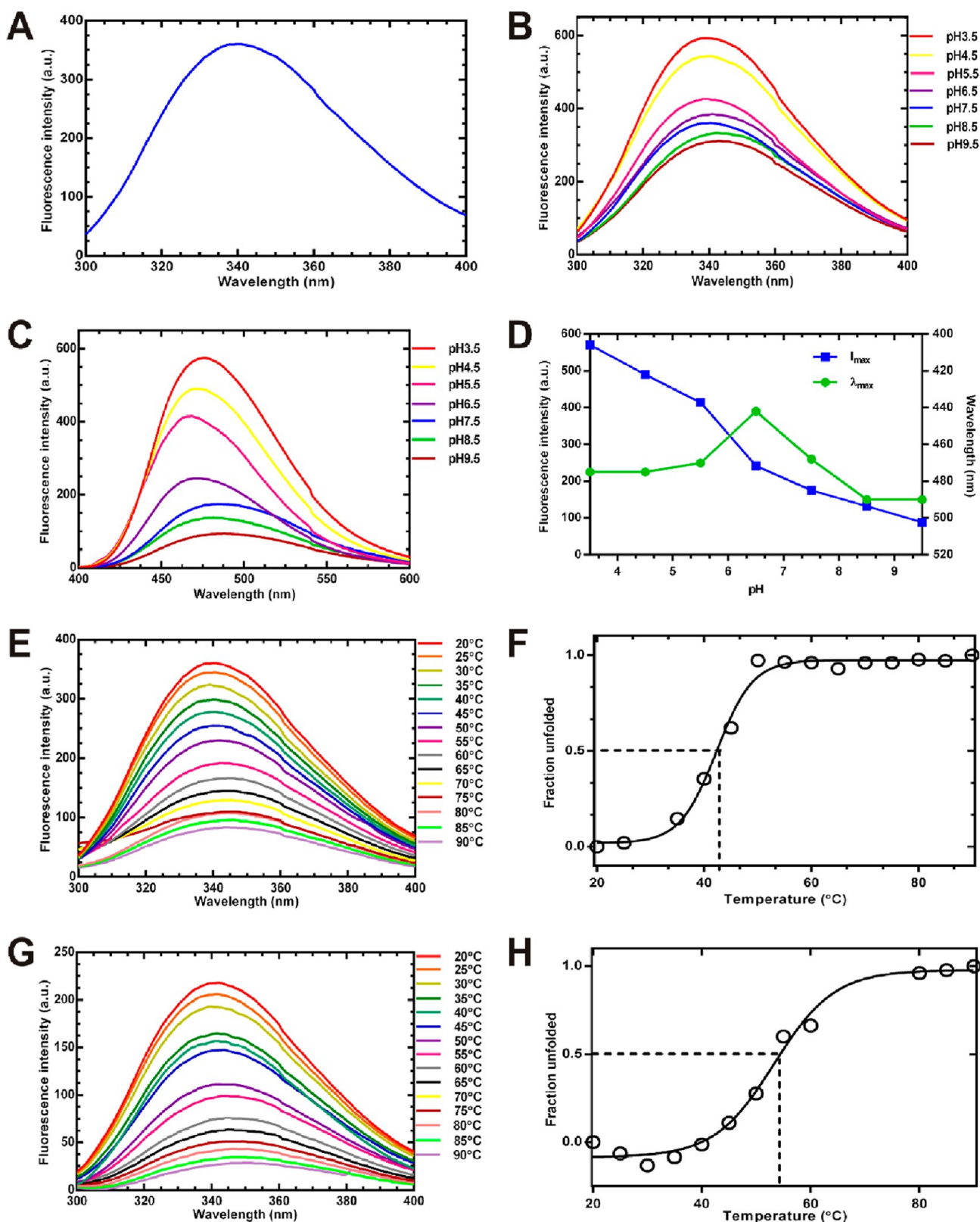
Figure 4. Fluorescence emission spectra of *Ld*RPE. Intrinsic fluorescence emission spectrum of *Ld*RPE at pH 7.5 (A) and different pH (B). Extrinsic fluorescence spectra of *Ld*RPE at various pHs with ANS (C). Fluorescence intensity and wavelength maxima as a function of pH (D). Effect of temperature on the emission spectra of apo (E) and complex of *Ld*RPE with the substrate (G) and their respective thermal-induced denaturation curves (F,H).

charged penetrates into the protein and exhibits the quenching effect on buried as well as surface tryptophan residues. However, potassium iodide is unable to penetrate into the protein due to its charge and shows a quenching effect on tryptophan residues present on the surface only. The quenching constants (K_{sv}) for acrylamide and KI were
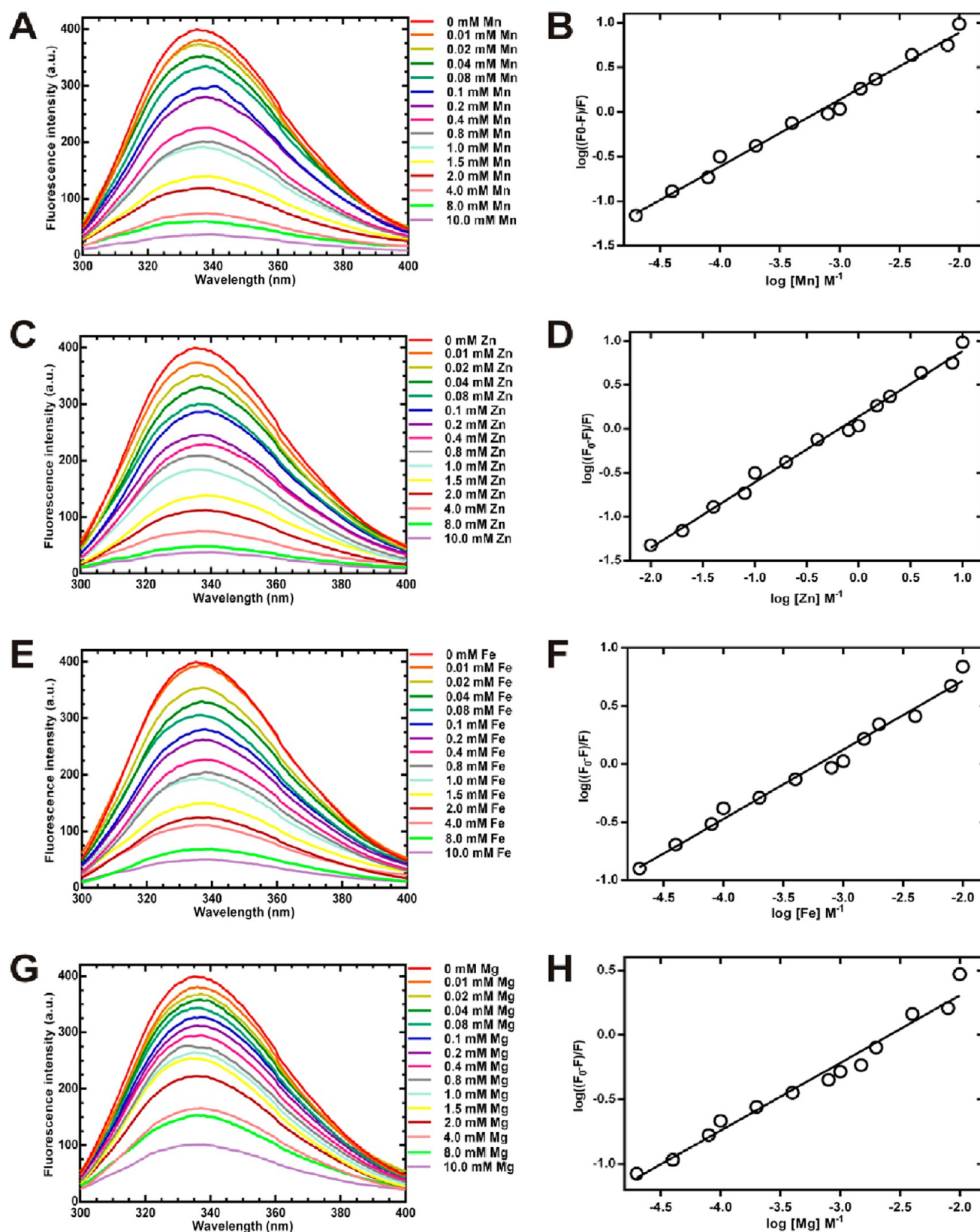
Figure 5. Intrinsic fluorescence study of *Ld*RPE with various divalent metal ions. Emission fluorescence spectra of *Ld*RPE with increasing concentration (0.01−10 mM) of Mn^{2+} (A), Zn^{2+} (C), Fe^{2+} (E), and Mg^{2+} (G) and their respective modified Stern−Volmer plot to enumerate the binding constant of Mn^{2+} (B), Zn^{2+} (D), Fe^{2+} (F), and Mg^{2+} (H).

determined using Stern−Volmer plot and found to be 5.077 ± 0.12 and 3.263 ± 0.16 M^{-1}, respectively (Figure 6B,D), which demonstrates more tryptophan residues to be buried rather than exposed to the solvent environment in *Ld*RPE. Simultaneously, unfolding studies of *Ld*RPE with urea showed a steady rise in fluorescence intensity with increasing

Table 2. Binding Constant Analysis with Various Divalent Ions

S. No.	Divalent ions	Binding constant (M^{-1})
1	Mn^{2+}	246 ± 7.1
2	Zn^{2+}	147.5 ± 6.1
3	Fe^{2+}	81.2 ± 2.9
4	Mg^{2+}	22.6 ± 1.3

concentration (up to 6.5 M) and reached saturation, depicting complete denaturation from 6.5 to 8 M urea (Figure 6E). Further, the data were normalized and fitted into a two-state equation in order to deduce the parameters such as free energy (ΔG) and mid transition concentration (C_m) that were found to be 3.0 ± 0.06 kcal mol^{-1} and 3.6 M, respectively (Figure 6F). Concurrently, LdRPE has shown higher ΔG (3.2 ± 0.06 kcal mol^{-1}) and C_m (4.0 M) in the presence of a substrate, delineating a moderate increase in tolerance to urea (Figure 6G).

2.6. Three-Dimensional Structure of LdRPE. The three-dimensional structure of LdRPE was generated without the first 26 amino acids of the N-terminus and last 14 amino acids of the C-terminus as there was no template available for these residues during BLASTp search. The LdRPE structure was comparatively modeled using the structural coordinates of *P. falciparum* RPE (PfRPE, PDB ID: 1TQX) as a template showing 44.4% identity, 67% similarity, 84% query coverage, and 6×10^{-63} e-value. Out of 10 generated models, the first structure was considered for further analysis on the basis of structural geometry and root mean square deviation (RMSD) from the template. After energy minimization of the selected LdRPE structure, subsequent analysis with the Ramachandran plot suggested 87.7% (168 residues) and 0% residues in most favored and disallowed regions, respectively, highlighting that the backbone dihedral angles, psi and phi, were considerably precise in the generated model. The overall quality factor of the final structure enumerated by ERRAT showed a value of 81.39 that denotes the proper arrangement of the non-bonded atomic interactions in the LdRPE model. Additionally, Verify3D illustrated 99.5% compatibility between its amino acid sequences (1D) and atomic model (3D) with an average 3D-1D score ≥ 0.2. The structural alignment of energy-minimized LdRPE with a template (PfRPE) showed an overall RMSD of 0.327 Å (for 191 paired Cα atoms), illustrating a close similarity between the two structures. The modeled structure exhibited all the characteristic features of the ribulose-phosphate family possessing $(\beta/\alpha)_8$ fold along with a regulating loop at the active site (Figure 7A). The LdRPE structure comprises a single domain (29−229 residues) with a classical triose phosphate isomerase (TIM) barrel $(\beta/\alpha)_8$ fold, whose core is composed of 8 stranded parallel sheets ($\beta1\uparrow$, $\beta2\uparrow$, $\beta3\uparrow$, $\beta4\uparrow$, $\beta5\uparrow$, $\beta6\uparrow$, $\beta7\uparrow$, $\beta8\uparrow$) folded in a cylindrical fashion to create a central active-site pocket. The central β-sheet is flanked by 11 α-helices ($\alpha1$ to $\alpha11$), which are conserved among all TIM-barrel folds. The residues Gly66 to Gly78 and Thr170 to Met181 formed respective loops 3 and 10 that are involved in capping the active site.

The active site of LdRPE consists of conserved residues Gly174, Phe175, Gly177, Gly205, Gly225, and Thr226 with majority of them being hydrophobic in nature. Interestingly, the active site pocket contains three methionines, namely, Met65, Met97, and Met169 in $\beta2$, $\beta3$, and $\beta6$ strands, respectively, which are well conserved in its orthologues

(PfRPE, ScRPE, EcRPE, and HsRPE) with an exception in TcRPE where Met65 is replaced by Ile60. The epimerization reaction earlier observed in RPE of potato chloroplasts highlighted that the residues Asp43, Asp185, His41, and His74 form hydrogen bonds, and the three methionine residues stabilize the substrate Ru5P to prevent isomerization and promote epimerization.[24] The residues involved in epimerization reaction are well-conserved in LdRPE, which indicates a similar epimerization pattern of the substrate in the leishmanial parasite. Moreover, the structure of LdRPE was superimposed on PfRPE (PDB ID: 1TQX) to study the metal binding site in the leishmanial enzyme. The superimposition deciphered the coordination of one divalent metal ion (Zn^{2+}) in the central active-site pocket and also revealed that the residues participating in metal binding were identical in LdRPE and PfRPE; particularly His61, Asp63, His95, and Asp203 formed an interaction with zinc ions (Figure 7B).

2.7. Dimerization of LdRPE. The dimeric structure of LdRPE possessing the lowest DOPE score as well as low RMSD against the template was selected from the output of the Modeller. The LdRPE dimer was shaped by the residues present between $\alpha1−\alpha2$ and $\beta2−\alpha3$ of both molecules, where its interface was stabilized by two salt bridges formed by Asp66-His68, His68-Asp66, and five polar contacts between Cys40-Gly43, Gly43-Cys40, His68-Ser99, Ser74-Gly76, and Gly76-Ser74 of molecules A and B (Figure 7C). The structural alignment of dimeric LdRPE with RPEs of other organisms depicted that leishmanial RPE has more structural resemblance to PfRPE with an RMSD of 0.618 Å, while the respective deviations were 1.117 and 1.041 Å for HsRPE and TgRPE from the LdPRE structure. Further analysis also revealed that the total number of salt bridges and polar contacts varied among RPE dimeric interfaces in various organisms; for instance, LdRPE and TgRPE showed five polar contacts each, but HsRPE and PfRPE exhibited 11 for each (Table 3).

Notably, salt bridges observed in LdRPE were also found to be conserved in the crystal structures of HsRPE and TgRPE, whereas aspartic acid was replaced by glutamic acid in PfRPE. In addition, PISA server delineated the buried surface area for LdRPE to be 939.8 Å^2 upon dimerization, whereas it was observed as 921.2, 1067.8, and 1140.3 Å^2 for TgRPE, HsRPE, and PfRPE, respectively. It suggests that the buried surface area for LdRPE was quite similar to that of the *Toxoplasma gondii* dimeric structure instead of PfRPE, which has been used to generate its structure. The binding affinity predicted by the PRODIGY server manifested that the affinities between two molecules of the dimer among RPE of these organisms are comparable, particularly LdRPE and TgRPE displayed identical values (-10.0 kcal mol^{-1}). Similarly, the dissociation constant of LdRPE (4.8×10^{-8} M) was found to be identical to that of TgRPE but lesser than that of PfRPE and HsRPE. It indicates that the dimer of LdRPE is less stable than those of PfRPE and HsRPE, which could be due to the differences in the number of residues involved in the interactions at the dimeric interface.

2.8. Assessment of Ligand-Binding to LdRPE. To obtain insights into ligand binding along with attributes of the interacting residues of LdRPE, the SwissDock server was employed, which exhibited a higher binding affinity of the enzyme for the substrate (Ru5P, -8.27 kcal mol^{-1}) in comparison to the product (Xu5P, -7.4 kcal mol^{-1}). The complex of LdRPE with Ru5P and Xu5P has revealed that ligands were bound deep inside a narrow tunnel just above the β-barrel of the enzyme (Figure 8A,C). The residues Gly177,
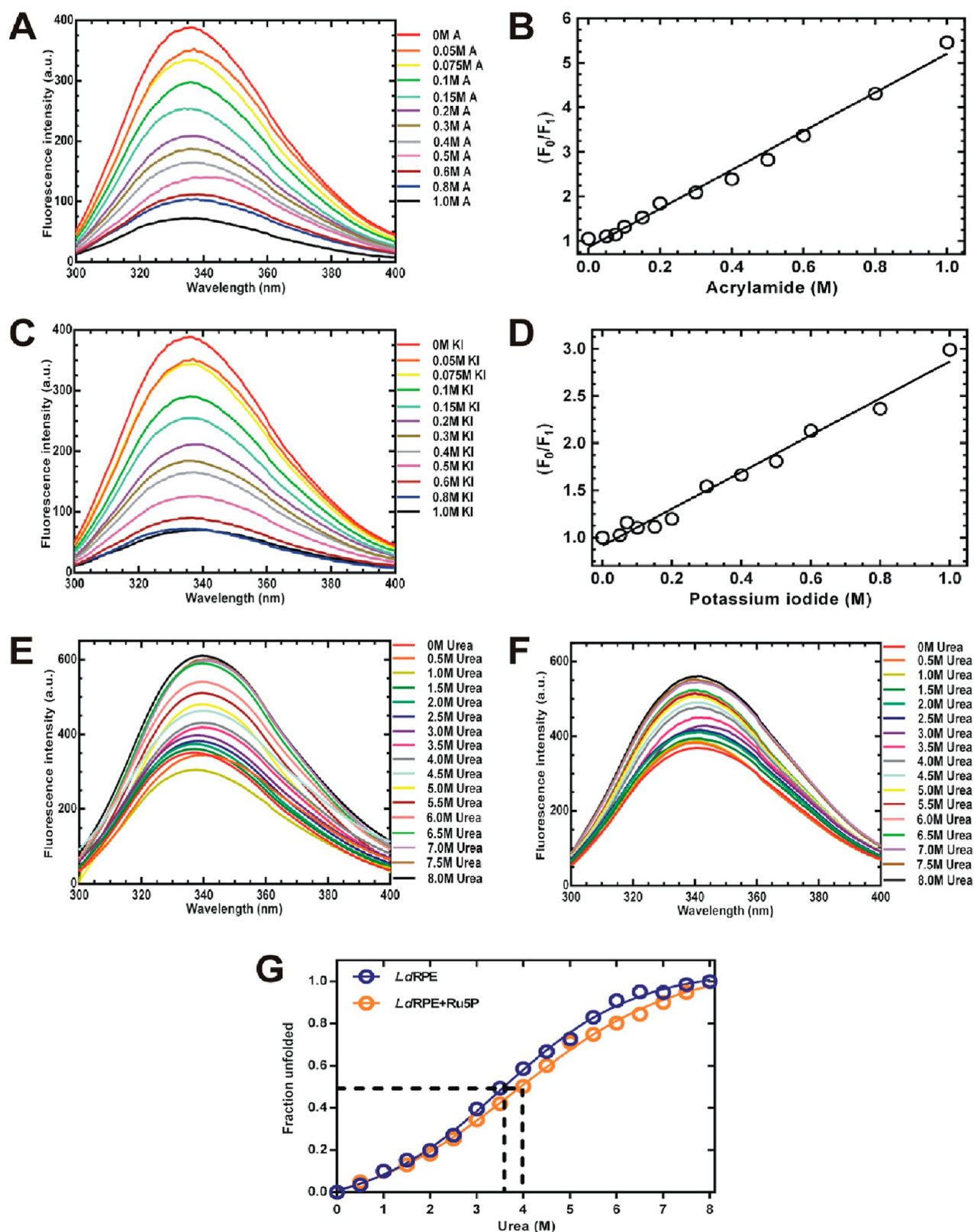
Figure 6. Intrinsic fluorescence quenching and unfolding studies of *Ld*RPE. Fluorescence spectra of *Ld*RPE with different concentrations (0−1 M) of acrylamide (A) and KI (C) and their respective Stern−Volmer plots enumerate the quenching constant (B,D). Effect of increasing urea concentration (0−8 M) on intrinsic fluorescence spectra of apo (E) and complex of *Ld*RPE with the substrate (F) and their unfolding plots (G) fitted into a two-state equation.

Gly205, Gly225, and Thr226 formed hydrogen bonds through their nitrogen atoms with the oxygen atoms of the Ru5P phosphate group, whereas the oxygen atom of Asp203

displayed an interaction with the hydrogen atom of the hydroxy group of the Ru5P ribulose moiety (Figure 8B). Similarly, Xu5P was also positioned in the substrate binding
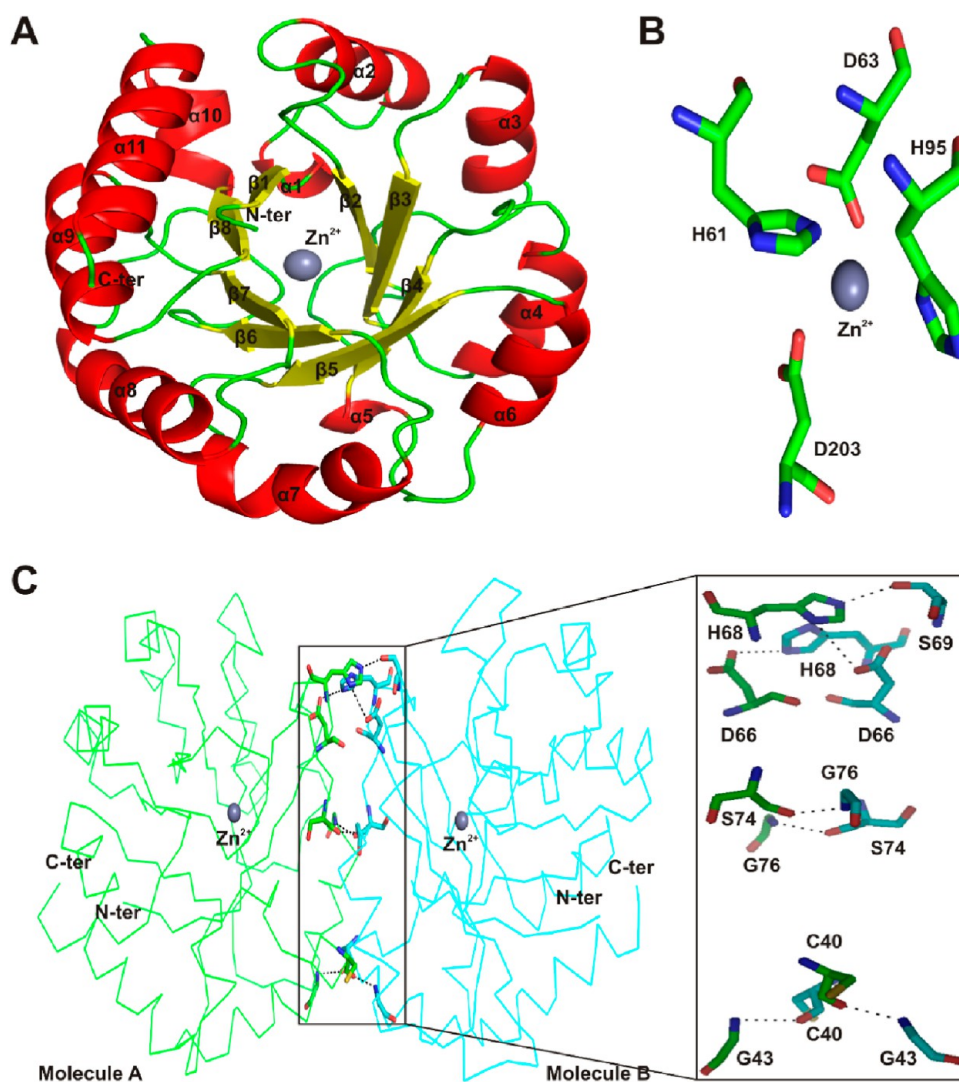
Figure 7. Modeled three-dimensional structure of *Ld*RPE. (A) Monomer of the 3D structure of *Ld*RPE is represented in cartoon form, where α-helices, β-strands, and random coils are shown in red, yellow, and green colors, respectively. Zinc metal ions present in the active site are displayed as gray colored circles. (B) Interacting residues of the Zn^{2+} binding site are labeled and denoted as green sticks and metal ions as gray circles. (C) Dimeric structure of *Ld*RPE contains two molecules shown in green and cyan colors with the inset depicting the interacting residues between two molecules labeled and represented as sticks, whereas black dashed lines indicate the intramolecular interactions.

pocket with the orientation similar to that of Ru5P, and the interaction analysis delineated the phosphate group of Xu5P to interact with the nitrogen atoms of Gly177, Gln178, Gly205, and Thr226 by hydrogen bonds, while Asp63 showed an interaction with the oxygen of the xylulose moiety (Figure 8D).

Interestingly, Gly177, Gly205, and Thr226 from loop11, loop13, and loop15 that are positioned between β6−α8, β7−α9, and β8−α10, respectively, were found to interact with the substrate as well as the product. Additionally, docking studies of substrate analogues (Comp A−E) showed that all compounds bind into the substrate binding pocket of *Ld*RPE with higher binding affinity as compared to Ru5P (Table 4).

Subsequent analysis of the protein-compound complex delineated that the substrate, Comp A, and Comp C−E form five hydrogen bonds with *Ld*RPE, while Comp B shows four such bonds (Figure 9A−F). Remarkably, Gly177, Gly205, and Thr226 were the common interacting residues forming hydrogen bonds with all the analogues. Among all the substrate

analogues, Comp C and E showed more binding affinity (−9.5 kcal mol^{-1}) toward *Ld*RPE.

2.9. Substrate Analogues form a Stable Complex with *Ld*RPE. Molecular dynamics simulation (MDS) was used to assess the stability of the *Ld*RPE structure in the presence of ligands including the substrate, product, and substrate analogues. The parameters such as RMSD, R_g, and root mean square fluctuation (RMSF) were employed for the analysis of its stability, compactness, and flexibility during MDS. The average RMSD evaluated for apo and complexes with the substrate, product, and Comp A-E were found to be 0.40, 0.36, 0.38, 0.35, 0.33, 0.49, 0.34, and 0.37 nm, respectively (Figure 10A). Overall deviations reduced moderately in complex structures as compared to that of the apo, except for the complex with Comp C.

The compactness of apo *Ld*RPE and the complex structures was analyzed by plotting R_g values against time, which revealed that the respective average R_g values of apo and complexes with the substrate, product, and Comp A−E were 1.63, 1.62, 1.63, 1.61, 1.69, 1.61, 1.68, and 1.65 nm, respectively (Figure 10B).

Table 3. Structural Comparison of the Leishmanial RPE Model with Other Organisms

|	_Ld_RPE	_Pf_RPE	_Tg_RPE[a]	_Hs_RPE
PDB ID	--	1TQX	4NU7	3OVQ
No. of residues	263	227	409	228
Sequence identity with _Ld_RPE	--	44.44%	42.26%	42.42%
RMSD (Å) vs _Ld_RPE	--	0.618	1.117	1.041
No. of salt bridges at the interface	2	2	4	2
No. of polar contacts between chains	5	11	5	11
Buried surface area (Å^2)	939.8	1140.3	921.2	1067.8
Binding affinity (kcal mol^{-1})	−10.0	−12.3	−10.0	−11.8
Dissociation constant (M)	4.3×10^{-8}	9.3×10^{-10}	4.8×10^{-8}	2.0×10^{-9}

[a]In the case of _Tg_RPE, a dimeric interface of A and C chains was extracted from the crystal structure (PDB ID: 4NU7) and employed for comparative analysis.

It highlighted negligible changes in the compactness of the protein in the presence of RuP5P, Xu5P, and compounds (A and C) in comparison to apo and other compounds.

Simultaneously, the flexibility of the protein during MDS was analyzed by enumerating the average RMSF values of apo and all the complexes with the substrate, product, and compounds (A−E) that were observed to be 0.16, 0.14, 0.15, 0.15, 0.15, 0.18, 0.17, and 0.17 nm, respectively (Figure 10C), revealing lower or negligible fluctuations in the backbone atoms of _Ld_RPE residues in the presence of all ligands except for Comp C. Additionally, the residues (Gly177, Gln178, Gly205, and Thr226) mainly involved in the interaction with ligands displayed a reduction in backbone atom fluctuation in comparison to that of the apo form of _Ld_RPE, particularly in the presence of ligands Ru5P, Xu5P, and the compounds (A, C, and E).
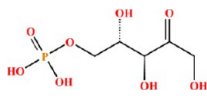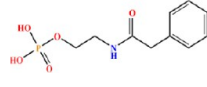
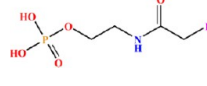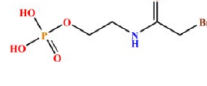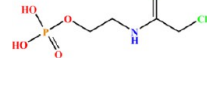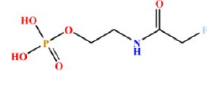## 3. DISCUSSION

The RPE enzyme participates in the reversible conversion of D-Ru5P to D-xylulose-5-phosphate during the first non-oxidative stage of the PPP. PPP is known to confer protection against oxidative stress and plays a crucial role in NADPH/NADP$^+$ homeostasis, which is also involved in the detoxification of the ROS.[4] In addition, the absence of functional RPE in _Saccharomyces cerevisiae_ resulted in sensitivity for oxidative stress.[14] Given that the RPE enzyme dispenses several crucial tasks in the leishmanial parasite, the present work highlights the cloning and purification of _Ld_RPE followed by biophysical
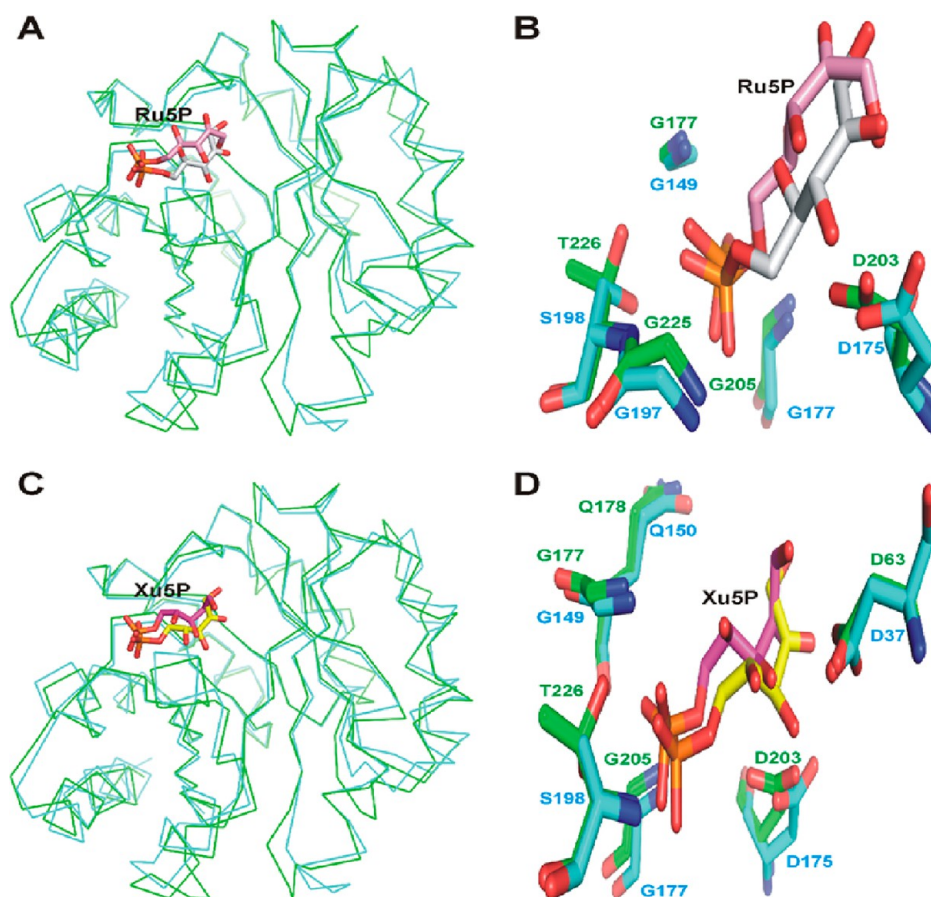
Figure 8. Interaction studies of _Ld_RPE with the substrate and product. Docked complexes of _Ld_RPE with ligands were generated using SwissDock and represented as green ribbons. Subsequently, crystal structures of human RPE (cyan color) bound with the substrate (PDB ID: 3OVQ) and product (PDB ID: 3OVR) were superimposed onto the respective structures of _Ld_RPE with Ru5P (A) and Xu5P (C) to compare the positions of the ligands. The residues of leishmanial and human RPEs interacting with Ru5P (B) and Xu5P (D) are labeled and displayed as green and cyan sticks, respectively.

Table 4. Binding Affinity of the Substrate and Its Analogues Complexed with Leishmanial RPE

Compound Id	Name of Compound	Binding Affinity (kcal mol^{-1})	Structure	Interacting residues
Ru5P	Ribulose-5-phosphate	-8.2		Gly177, Gly205, Gly225, Asp203, Thr226
Comp A	2-(2-phenylacetamido)ethyl dihydrogen phosphate	-8.5		Gly177, Gln178, Gly205, Ile206, Thr226
Comp B	2-(2-iodoacetamido)ethyl dihydrogen phosphate	-9.2		Gly177, Gln178, Gly205, Thr226
Comp C	2-(2-bromoacetamido)ethyl dihydrogen phosphate	-9.5		Gly177, Gln178, Gly205, Ile206, Thr226
Comp D	2-(2-chloroacetamido)ethyl dihydrogen phosphate	-8.96		Gly177, Gln178, Gly205, Asp203, Thr226
Comp E	2-(2-fluoroacetamido)ethyl dihydrogen phosphate	-9.5		Gly177, Gln178, Gly205, Ile206, Thr226

and structural characterization. Similar to other members of epimerases belonging to the "ribulose phosphate binding" superfamily, *Ld*RPE contains a single domain exhibiting conserved phosphate binding residues and a typical $(\beta/\alpha)_8$ TIM architecture that along with a loop plays a role in regulating the access to the active site.[8] A conserved active site is observed in *Ld*RPE, similar to the orthologues of RPEs of different organisms, while threonine is present in leishmanial RPE instead of serine in its human counterpart. Notably, the N-terminal extension of trypanosomatid parasites does not correspond to its equivalents in other organisms. In addition, a unique insertion of three amino acids was found near the N-terminus of RPEs of trypanosomatids that is not present in higher eukaryotes including human and yeast. Furthermore, purified *Ld*RPE is present as a homodimer in solution form, which is in agreement with the earlier reports of RPEs from rice[7] and *P. falciparum*;[11] on the contrary, RPEs are reported to assemble as hexamers in *Cyanobacterium synechocystis*[25] and *Streptococcus pyogenes*.[12]

The life cycle of the leishmanial parasite encompasses the promastigote and amastigote stages, enduring the change in temperature as well as pH. The variation in conditions elicits

development of the parasite in the vector[26] causing parasitic proteins to undergo conformational changes to adapt to the altered environments. Thus, information of the physical properties of various leishmanial proteins and their possible synergistic effects in the maintenance and propagation of the parasite at a particular stage becomes highly significant. The biophysical studies revealed that *Ld*RPE possesses adequate secondary structural elements with a predominately alpha helical content at physiological pH, which is in accordance with other leishmanial enzymes including PP1[27] and PepT.[28] Remarkably, the secondary structure observed in *Ld*RPE was comparable to crystal structures of RPEs from *P. falciparum*,[11] *T. gondii*,[29] and *H. sapiens*.[8] The melting temperature (T_m) of *Ld*RPE has indicated cooperative unfolding, which is similar to that of previously reported in leishmanial protein phosphatase 2C.[30] Further, the secondary structure of *Ld*RPE revealed a moderate stability with no significant changes at lower concentrations of urea but complete loss in ellipticity at its higher levels. It is in corroboration with the earlier studies on the alanyl-tRNA synthetase from *E. coli*[31] and the aspartyl-tRNA synthetase from *L. donovani*.[32] Tryptophan fluorescence is widely used to probe the structural changes of protein during
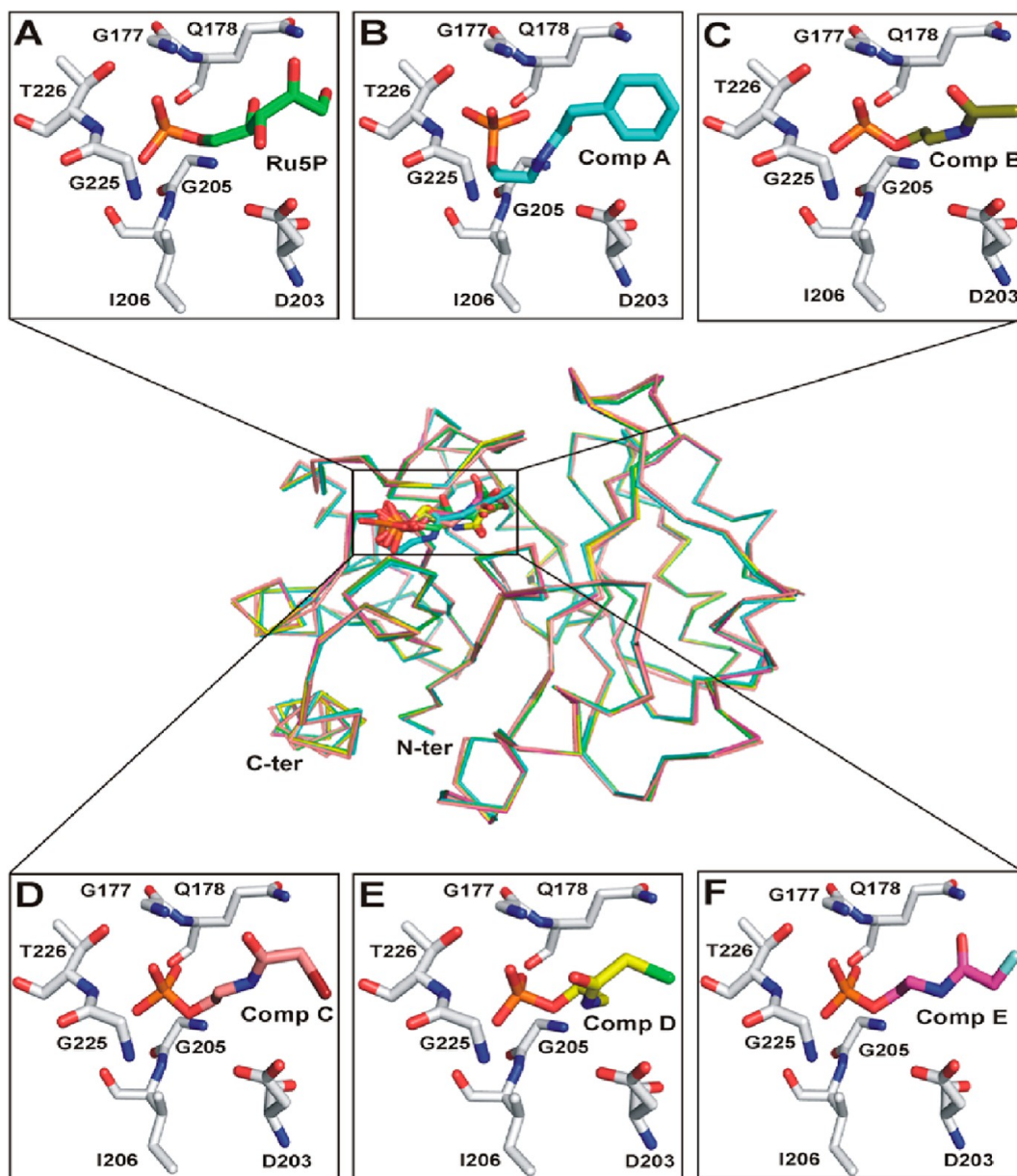
Figure 9. Molecular docking of *Ld*RPE with the substrate and its analogues. *Ld*RPE was docked with the substrate and its analogues followed by their alignment to reveal the interacting residues. The residues of *Ld*RPE interacting with Ru5P (A), Com A (B), Com B (C), Com C (D), Com D (E), and Com E (F) are presented as gray sticks and labeled.

unfolding,[33] and it indicates that tryptophan residues of *Ld*RPE are located in a relatively hydrophobic milieu with only a small fraction on the protein surface. Subsequently, quenching experiments confirmed the tryptophan residues to be majorly buried inside the core of the enzyme, and a similar phenomenon has also been observed in the modeled *Ld*RPE structure. The ANS binding study of *Ld*RPE revealed aggregation at acidic pH in comparison to the protein at neutral pH, which was also reported in other leishmanial proteins such as PdxK[34] and 6PGDH.[35] The uncharged urea molecules have more tendency to bind the unfolded state of the protein as compared to the folded one;[36] our study has also represented the two-state transition of *Ld*RPE with urea that gradually leads to unfolding.

The three-dimensional structure of *Ld*RPE represents all common topological features as observed in previously reported RPE crystal structures of *P. falciparum*[11] and *H.*

sapiens.[8] Similarly, the dimeric structure of *Ld*RPE and its interface were found to be comparable to other RPE structures from *T. gondii*,[27] *P. falciparum*,[11] and human,[8] showing a similar arrangement of molecules and number of salt bridges along with participating residues, particularly aspartic acid and histidine. Further analysis of molecular interactions of *Ld*RPE with the substrate and product revealed that it possesses a single binding pocket for the substrate and product, which was also reported in the crystal structure of its counterpart in human.[8] Recently, Gonzalez and co-workers[37] identified substrate (Ru5P)-analogue derivatives, compounds A–E and found that these compounds inhibit RPI-B of *T. cruzi* through a competitive mode of action. Since RPI-B is a competitor enzyme of RPE and also utilizes Ru5P as a substrate, molecular docking studies of *Ld*RPE with these inhibitors revealed them to be fitting in the substrate-binding pocket with higher binding affinity than the substrate (Ru5P), advocating that the
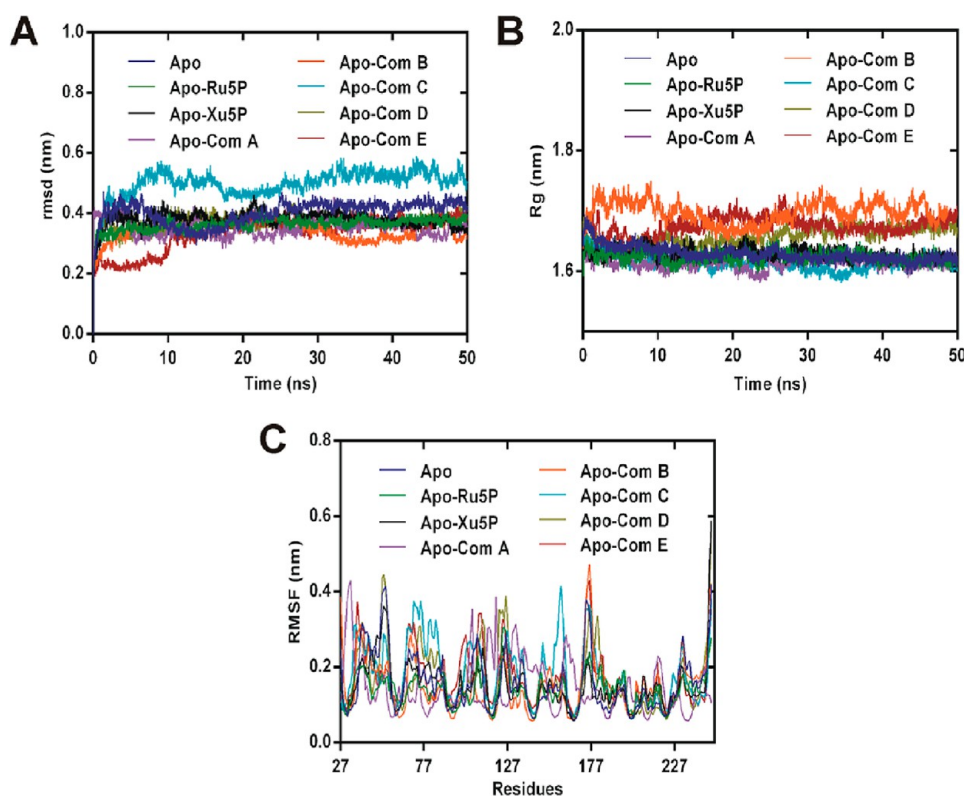
Figure 10. MDS of apo *Ld*RPE and its complexes. The plots display RMSD (A), R_g (B), and RMSF (C) for apo *Ld*RPE and its docked complexes with Ru5P, Xu5P, Com A, Com B, Com C, Com D, and Com E.

mode of inhibition is competitive. In corroboration with the previous *in vitro* study,[37] Comp B displays a better binding affinity toward leishmanial RPE in comparison to the substrate. The stability, flexibility, and compactness of *Ld*RPE in the presence of substrate analogues (Comp A−E) were found to be better than the apo as well as complexes with the substrate and product, which delineated a stable interaction of the respective compounds in the binding pocket. Concurrently, the conserved active site residues, that is, glycine and threonine, also exhibited lesser fluctuation in the complex when compared to the apo form. Nevertheless, investigation and evaluation of more substrate analogues of RPEs could facilitate the reinforcement of our knowledge toward the development of next-generation inhibitors that can potentially act as anti-leishmanial agents.

4. CONCLUSIONS

The present study provides the first report on biophysical and structural attributes of RPE from leishmanial parasites. *Ld*RPE comprises a single domain that harbors conserved catalytic residues and two peculiar trypanosomatid-specific insertions at the N-terminus. Leishmanial RPE was purified to homogeneity and observed as a homodimer in the solution with more alpha helical content at physiological pH as observed in RPEs of other organisms. Most of the tryptophan residues of *Ld*RPE are inaccessible to solvents and buried in the hydrophobic region, while an unfolding study with urea delineates the enzyme to be moderately tolerant for urea. Furthermore, the three-dimensional model of leishmanial RPE displays significant structural similarity with its orthologue in *P. falciparum* and human and also reveals a sole binding pocket for the substrate as well as the product. Remarkably, *Ld*RPE exhibits a

higher binding affinity toward the substrate analogues than the substrate with their placement into a substrate-binding site, suggesting a competitive mode of inhibition. Furthermore, *Ld*RPE complexes with the substrate, product, and substrate analogues were found to be more stable in comparison to the apo form during simulation. Therefore, our study has provided important insights into the structural basis of inhibition by substrate analogues that could be further explored for developing novel and specific therapeutic interventions to combat leishmaniasis.

5. METHODS

5.1. Sequence and Phylogenetic Analysis. The protein sequence of *Ld*RPE (XP_003863992) was retrieved from the NCBI database (https://www.ncbi.nlm.nih.gov/protein) and submitted to ProtParam (https://web.expasy.org/protparam/) and TOPCONS (http://topcons.cbr.su.se/) tools for sequence analysis. Simultaneously, the multiple sequence alignment was carried out for the different organisms such as *T. cruzi* (XP_804346), *P. falciparum* (XP_001350598), *H. sapiens* (NP_954699), and *L. donovani* (XP_003863992) by the Clustal Omega alignment tool (https://www.ebi.ac.uk/Tools/msa/clustalo/) to understand the sequence homology and residues involved in binding with the substrate and product. Further, a phylogenetic study of *Ld*RPE was carried out with various organisms, and protein sequences used in this analysis were retrieved from the GenBank database (http://www.ncbi.nlm.nih.gov/entrez/query.fcgi?db=Protein). A phylogenetic tree was constructed using MEGA-X software (https://www.megasoftware.net/) with the neighbor-joining method by taking default parameters with the 1000 bootstrap test and *p*-distance method of evaluation.

5.2. Molecular Cloning and Protein Purification. A full-length *Ld*RPE ORF of 792 nucleotides (Gene ID: 13392387; https://www.ncbi.nlm.nih.gov/gene) was amplified from genomic DNA of *L. donovani* (Strain: MHOM/IN/80/DD8) using gene specific forward (5′ AAT <u>CAT ATG</u> ACG GAG TTC AAC CGC TAC AAC 3′) and reverse (5′ AAT <u>GAA TTC</u> TTA CCT CGT CCC TGG TAG CGC 3′) primers with *Nde*I and *Eco*RI restriction sites. The amplicon was digested using *Nde*I and *Eco*RI and ligated into a pET28a (+) expression vector that incorporates a hexa-histidine tag to the N-terminus of recombinant protein. Subsequently, positive clones were confirmed through restriction digestion succeeded by DNA sequencing. The positive clone was transformed into *E. coli* BL21 (DE3) cells, and a single colony of the *Ld*RPE construct was grown in Luria−Bertani (LB) broth supplemented with kanamycin (50 μg mL^{-1}) at 37 °C for 16−18 h. Next day, the primary culture was inoculated into 750 mL of LB broth with kanamycin (50 μg mL^{-1}) at 37 °C till the OD$_{600nm}$ reaches 0.5−0.6. Further, 0.4 mM isopropylthio-β-galactoside was added, and then cells were grown for 18−20 h at 18 °C in a shaking incubator followed by centrifugation at 7000 rpm for 10 min. The cell pellet was suspended in 35 mL of lysis buffer [20 mM HEPES pH 7.5, 300 mM KCl, 2 mM β-ME, 1 mM PMSF, lysozyme (0.25 μg mL^{-1})] under continuous stirring at 4 °C for 1 h and sonicated at 35% amplitude for 30 min with 10 s on/off cycles. The sonicated sample was centrifuged at 12,000 rpm for 30 min at 4 °C, and the resultant supernatant was filtered and injected into the HisTrap HP 5 mL column (GE Healthcare) equilibrated using Buffer-A (20 mM HEPES pH 7.5, 300 mM KCl, and 18 mM imidazole). After washing with Buffer-A, the His-tagged protein was eluted using Buffer-B containing 20 mM HEPES pH 7.5, 300 mM KCl, and 300 mM imidazole. Protein fractions were loaded on the 10% SDS-PAGE gel, and fractions containing pure protein were pooled followed by concentration using a Centricon of 10 kDa cut-off. To determine the oligomeric form of the purified protein, the concentrated fraction was loaded onto the Superdex 16/600 200 pg column (GE Healthcare) equilibrated with a buffer comprising 20 mM HEPES pH 7.5 and 100 mM KCl. The molecular weight of the purified *Ld*RPE was enumerated employing the calibration curve of standard proteins. Finally, the concentration of *Ld*RPE was measured through NanoDrop 2000c using the molar extinction coefficient and molecular weight as 24,240 M^{-1} cm^{-1} and 31,236.04 Da, respectively.

5.3. CD Measurements. Secondary structural elements of recombinant *Ld*RPE were assessed using a CD spectrophotometer (JASCO 1500) equipped with a Peltier-type temperature controller. The CD spectra were recorded in the far UV range (190−260 nm) using a quartz cell of path length of 2.0 mm, scanning speed of 20 nm min^{-1}, and protein concentration of 10 μM. The change in the secondary structural elements of *Ld*RPE was recorded in buffer (pH 3.5 to 9.5) containing 100 mM KCl, and the data were analyzed using the DichroWeb server (http://dichroweb.cryst.bbk.ac.uk). The Gibbs free energy of unfolding (ΔG) was calculated by denaturing the protein using various concentrations of urea (100 mM to 8 M), and the spectra were recorded between 250 and 220 nm. Simultaneously, thermal denaturation was executed by continuous evaluation of ellipticity at 222 nm at the temperature ranging from 20 to 90 °C with a linear increment of 1 °C min^{-1}. All experiments were performed in triplicate, and the data were fitted using the SigmaPlot 12.0.

5.4. Intrinsic Fluorescence Spectroscopy. The intrinsic fluorescence emission spectra of *Ld*RPE were collected using a Jasco spectrofluorometer (FP-8500) at 25 °C using a cuvette of 10 mm path length. The protein was excited at 280 nm, and the emission was measured from 300 to 400 nm, while a scanning speed of 100 nm min^{-1} was used for fluorescence experiments. The fluorescence study was performed with different buffers (pH 3.5-9.5) to establish the folding dynamics of *Ld*RPE in the native state. Simultaneously, the thermal stability of the protein with and without the substrate was analyzed with increasing temperature from 20 to 90 °C. Simultaneously, the purified protein (5 μM) was incubated with 2 mM substrate (Ru5P) on ice for 30 min followed by recording of spectra with every 5 °C interval using Peltier. Additionally, a hydrophobic cluster binding dye, ANS, was employed to observe the unfolding of *Ld*RPE at various pH. The *Ld*RPE protein was initially incubated with 25-fold higher ANS at room temperature in the dark for 30 min followed by excitation at 380 nm and emission from 400 to 600 nm. Simultaneously, the location of tryptophan residues in *Ld*RPE was also projected using the WESA online server (https://pipe.rcc.fsu.edu/wesa/). Furthermore, the effect of quenching agents (acrylamide and potassium iodide) and the denaturant compound (urea) on *Ld*RPE was studied through intrinsic fluorescence measurements. The protein and different concentrations of quenching agents (0 to 1.0 M) were incubated for 1 h, and the emission spectra were recorded from 300 to 400 nm. Subsequently, urea was also employed for unfolding study of *Ld*RPE in the presence of the substrate as well as in apo form. Initially, the *Ld*RPE protein was incubated for 30 min with a saturation concentration of the substrate (5 mM Ru5P) followed by addition of urea (0 to 8.0 M). The emission spectra were observed after 1 hr and the Gibbs free energy (ΔG) was enumerated using the two-state equation.

In addition, the fluorescence quenching data were analyzed using the Stern−Volmer plot with a quencher concentration on the X-axis and F_o/F_1 on the Y-axis, while the Gibbs free energy (ΔG) was calculated using the two-state equation. In order to determine the binding constants of different divalent metals with *Ld*RPE, stocks of Zn, Mn, Fe, and Mg ions were freshly prepared in 20 mM HEPES pH 7.5 and 100 mM KCl. *Ld*RPE was incubated with varying concentrations of divalent metals from 0 to 10 mM for 30 min at room temperature followed by fluorescence spectra measurement. The binding constant (K_a) was determined using a modified Stern−Volmer equation, that is, $\log(F_0 - F)/F = \log K_a + n \log[Q]$, where F_0 and F are the intensities of the protein in the absence and presence of the ligand, respectively, and Q is the divalent metal concentration. All the fluorescence measurements were performed in triplicate, and their respective blank corrections were made.

5.5. Homology Modeling. BLASTp was performed against PDB to identify a suitable template to generate the three-dimensional structure of *Ld*RPE through homology modeling. The structure of *P. falciparum* RPE (PDB ID: 1TQX) was selected as a template to model the monomer and dimer of leishmanial RPE. Subsequently, Modeller 9.25 version[38] was employed to generate the structure of *Ld*RPE using the designated template, and the best model was selected based on its DOPE score followed by assessment of stereochemical properties using PROCHECK[39] of SAVES v6.0 (https://saves.mbi.ucla.edu/). The selected structure was subjected to energy-minimization using the GROMACS 5.1.4

package,[40] and its structural quality was evaluated using the Ramchandran plot, ERRAT,[41] and Verify 3D[42] programs available on SAVES v6.0 (https://saves.mbi.ucla.edu/). To understand the dimeric interface of *Ld*RPE, interactions between two molecules were analyzed using PyMol (https://pymol.org/2/) and PIC (http://pic.mbu.iisc.ernet.in/). PRODIGY (https://wenmr.science.uu.nl/prodigy/) was employed to predict the binding affinity and dissociation constant of the dimeric interface, while the PISA server (https://www.ebi.ac.uk/pdbe/pisa/) was used to calculate the buried surface area upon dimerization.

5.6. Molecular Docking Studies. In order to find out the molecular interactions of the leishmanial protein with the substrate and product, molecular docking of the energy-minimized *Ld*RPE model was performed using the SwissDock server.[43] The structural coordinates of the substrate (Ru5P) and product (Xu5P) were obtained from the Ligand Expo server (http://ligand-expo.rcsb.org/ld-search.html). Simultaneously, a series of Ru5P analogues (Comp A−E) was constructed using Avogadro software (https://avogadro.cc/), and the coordinate files of the ligands were used on SwissDock server for docking in the active site of *Ld*RPE. A total of 20 docked complexes of each of *Ld*RPE bound substrate, product and Comp A−E were generated and the conformers with the higher binding affinity were used for further analysis.

5.7. Molecular Dynamics Simulations. MDS of apo *Ld*RPE and its complexes were performed by GROMACS employing GROMOS96 43a1 as a force field in a cubic box and an SPC water model according to a previous report.[44] The topology files of ligands generated by the PRODRG server (http://prodrg1.dyndns.org/) were amalgamated to form a complex topology file. The simulation system was neutralized by adding the suitable number of Na^+/Cl^- ions. Moreover, the steepest descent method was used to energy-minimize the solvated system in 50,000 steps for the stability and removal of steric clashes. After equilibrating the systems at 1 bar pressure and 300 K for 100 ps, production simulation was run for 50 ns to analyze the dynamics of each system. Subsequently, RMSD, radius of gyration (R_g), and RMSF were enumerated for apo *Ld*RPE and its complexes.

◼ AUTHOR INFORMATION

Corresponding Author

Insaf Ahmed Qureshi − *Department of Biotechnology & Bioinformatics, School of Life Sciences, University of Hyderabad, Hyderabad 500046, India;* ⓞ orcid.org/0000-0001-7720-7067; Phone: +91-40-23134588; Email: insaf@uohyd.ac.in

Authors

Bandigi Narsimulu − *Department of Biotechnology & Bioinformatics, School of Life Sciences, University of Hyderabad, Hyderabad 500046, India*

Rahila Qureshi − *Private Location, Hyderabad 500019, India*

Pranay Jakkula − *Department of Biotechnology & Bioinformatics, School of Life Sciences, University of Hyderabad, Hyderabad 500046, India*

Sayanna Are − *Department of Biotechnology & Bioinformatics, School of Life Sciences, University of Hyderabad, Hyderabad 500046, India*

Complete contact information is available at:
https://pubs.acs.org/10.1021/acsomega.1c04967

◼ ACKNOWLEDGMENTS

◼ REFERENCES

(1) Desjeux, P. Leishmaniasis: current situation and new perspectives. *Comp. Immunol. Microbiol. Infect. Dis.* **2004**, *27*, 305−318.

(2) Rodriguez-Contreras, D.; Aslan, H.; Feng, X.; Tran, K.; Yates, P. A.; Kamhawi, S.; Landfear, S. M. Regulation and biological function of a flagellar glucose transporter in Leishmania mexicana: a potential glucose sensor. *FASEB J.* **2015**, *29*, 11−24.

(3) Chang, K. P.; Dwyer, D. Leishmania donovani. Hamster macrophage interactions in vitro: cell entry, intracellular survival, and multiplication of amastigotes. *J. Exp. Med.* **1978**, *147*, 515−530.

(4) Barrett, M. The pentose phosphate pathway and parasitic protozoa. *Parasitol. Today* **1997**, *13*, 11−16.

(5) Stincone, A.; Prigione, A.; Cramer, T.; Wamelink, M. M. C.; Campbell, K.; Cheung, E.; Olin-Sandoval, V.; Grüning, N. M.; Krüger, A.; Tauqeer Alam, M.; Keller, M. A.; Breitenbach, M.; Brindle, K. M.; Rabinowitz, J. D.; Ralser, M. The return of metabolism: biochemistry and physiology of the pentose phosphate pathway. *Biol. Rev. Cambridge Philos. Soc.* **2015**, *90*, 927−963.

(6) Bär, J.; Naumann, M.; Reuter, R.; Kopperschläger, G. Improved purification of ribulose 5-phosphate 3-epimerase from Saccharomyces cerevisiae and characterization of the enzyme. *Bioseparation* **1996**, *6*, 233−241.

(7) Jelakovic, S.; Kopriva, S.; Süss, K. H.; Schulz, G. E. Structure and catalytic mechanism of the cytosolic D-ribulose-5-phosphate 3-epimerase from rice. *J. Mol. Biol.* **2003**, *326*, 127−135.

(8) Liang, W.; Ouyang, S.; Shaw, N.; Joachimiak, A.; Zhang, R.; Liu, Z. J. Conversion ofd-ribulose 5-phosphate toD-xylulose 5-phosphate: new insights from structural and biochemical studies on human RPE. *FASEB J.* **2011**, *25*, 497−504.

(9) Le, S. B.; Heggeset, T. M. B.; Haugen, T.; Nærdal, I.; Brautaset, T. 6-Phosphofructokinase and ribulose-5-phosphate 3-epimerase in methylotrophic Bacillus methanolicus ribulose monophosphate cycle. *Appl. Microbiol. Biotechnol.* **2017**, *101*, 4185−4200.

(10) Gonzalez, S. N.; Valsecchi, W. M.; Maugeri, D.; Delfino, J. M.; Cazzulo, J. J. Structure, kinetic characterization and subcellular localization of the two ribulose 5-phosphate epimerase isoenzymes from Trypanosoma cruzi. *PLoS One* **2017**, *12*, No. e0172405.

(11) Caruthers, J.; Bosch, J.; Buckner, F.; Van Voorhis, W.; Myler, P.; Worthey, E.; Mehlin, C.; Boni, E.; DeTitta, G.; Luft, J.; Lauricella, A.; Kalyuzhniy, O.; Anderson, L.; Zucker, F.; Soltis, M.; Hol, W. G. J. Structure of a ribulose 5-phosphate 3-epimerase from Plasmodium falciparum. *Proteins* **2006**, *62*, 338−342.

(12) Akana, J.; Fedorov, A. A.; Fedorov, E.; Novak, W. R. P.; Babbitt, P. C.; Almo, S. C.; Gerlt, J. A. d-Ribulose 5-Phosphate 3-Epimerase: Functional and Structural Relationships to Members of the Ribulose-Phosphate Binding $(\beta/\alpha)8$-Barrel Superfamily. *Biochemistry* **2006**, *45*, 2493−2503.

(13) Sobota, J. M.; Imlay, J. A. Iron enzyme ribulose-5-phosphate 3-epimerase in Escherichia coli is rapidly damaged by hydrogen

peroxide but can be protected by manganese. *Proc. Natl. Acad. Sci. U.S.A.* **2011**, *108*, 5402−5407.

(14) Tan, S.-X.; Teo, M.; Lam, Y. T.; Dawes, I. W.; Perrone, G. G. Cu, Zn Superoxide Dismutase and NADP(H) Homeostasis Are Required for Tolerance of Endoplasmic Reticulum Stress in Saccharomyces cerevisiae. *Mol. Biol. Cell* **2009**, *20*, 1493−1508.

(15) Hannaert, V.; Bringaud, F.; Opperdoes, F. R.; Michels, P. A. Evolution of energy metabolism and its compartmentation in Kinetoplastida. *Kinetoplastid Biol. Dis.* **2003**, *2*, 11.

(16) Opperdoes, F. R.; Coombs, G. H. Metabolism of Leishmania: proven and predicted. *Trends Parasitol.* **2007**, *23*, 149−158.

(17) Maugeri, D. A.; Cazzulo, J. J.; Burchmore, R. J. S.; Barrett, M. P.; Ogbunude, P. O. J. Pentose phosphate metabolism in Leishmania mexicana. *Mol. Biochem. Parasitol.* **2003**, *130*, 117−125.

(18) Cronín, C. N.; Nolan, D. P.; Paul Voorheis, H. The enzymes of the classical pentose phosphate pathway display differential activities in procyclic and bloodstream forms of Trypanosoma brucei. *FEBS Lett.* **1989**, *244*, 26−30.

(19) Alsford, S.; Turner, D. J.; Obado, S. O.; Sanchez-Flores, A.; Glover, L.; Berriman, M.; Hertz-Fowler, C.; Horn, D. High-throughput phenotyping using parallel sequencing of RNA interference targets in the African trypanosome. *Genome Res.* **2011**, *21*, 915−924.

(20) Kovářová, J.; Barrett, M. P. The Pentose Phosphate Pathway in Parasitic Trypanosomatids. *Trends Parasitol.* **2016**, *32*, 622−634.

(21) Allen, S. M.; Lim, E. E.; Jortzik, E.; Preuss, J.; Chua, H. H.; MacRae, J. I.; Rahlfs, S.; Haeussler, K.; Downton, M. T.; McConville, M. J.; Becker, K.; Ralph, S. A. Plasmodium falciparum glucose-6-phosphate dehydrogenase 6-phosphogluconolactonase is a potential drug target. *FEBS J.* **2015**, *282*, 3808−3823.

(22) Loureiro, I.; Faria, J.; Santarem, N.; Smith, T. K.; Tavares, J.; Cordeiro-da-Silva, A. Potential Drug Targets in the Pentose Phosphate Pathway of Trypanosomatids. *Curr. Med. Chem.* **2019**, *25*, 5239−5265.

(23) Haeussler, K.; Berneburg, I.; Jortzik, E.; Hahn, J.; Rahbari, M.; Schulz, N.; Preuss, J.; Zapol'skii, V. A.; Bode, L.; Pinkerton, A. B.; Kaufmann, D. E.; Rahlfs, S.; Becker, K. Glucose 6-phosphate dehydrogenase 6-phosphogluconolactonase: characterization of the Plasmodium vivax enzyme and inhibitor studies. *Malar. J.* **2019**, *18*, 22.

(24) Kopp, J.; Kopriva, S.; Süss, K.-H.; Schulz, G. E. Structure and mechanism of the amphibolic enzyme D-ribulose-5-phosphate 3-epimerase from potato chloroplasts. *J. Mol. Biol.* **1999**, *287*, 761−771.

(25) Wise, E. L.; Akana, J.; Gerlt, J. A.; Rayment, I. Structure of D-ribulose 5-phosphate 3-epimerase from Synechocystis to 1.6 Å resolution. *Acta Crystallogr., Sect. D: Biol. Crystallogr.* **2004**, *60*, 1687−1690.

(26) Bates, P.; Rogers, M. New insights into the developmental biology and transmission mechanisms of Leishmania. *Curr. Mol. Med.* **2004**, *4*, 601−609.

(27) Qureshi, R.; Jakkula, P.; Sagurthi, S. R.; Qureshi, I. A. Protein phosphatase 1 of Leishmania donovani exhibits conserved catalytic residues and pro-inflammatory response. *Biochem. Biophys. Res. Commun.* **2019**, *516*, 770−776.

(28) Bhat, S. Y.; Qureshi, I. A. Mutations of key substrate binding residues of leishmanial peptidase T alter its functional and structural dynamics. *Biochim. Biophys. Acta, Gen. Subj.* **2020**, *1864*, 129465.

(29) Lykins, J. D.; Filippova, E. V.; Halavaty, A. S.; Minasov, G.; Zhou, Y.; Dubrovska, I.; Flores, K. J.; Shuvalova, L. A.; Ruan, J.; El Bissati, K.; Dovgin, S.; Roberts, C. W.; Woods, S.; Moulton, J. D.; Moulton, H.; McPhillie, M. J.; Muench, S. P.; Fishwick, C. W. G.; Sabini, E.; Shanmugam, D.; Roos, D. S.; McLeod, R.; Anderson, W. F.; Ngô, H. M. CSGID Solves Structures and Identifies Phenotypes for Five Enzymes in Toxoplasma gondii. *Front. Cell. Infect. Microbiol.* **2018**, *8*, 352.

(30) Jakkula, P.; Qureshi, R.; Iqbal, A.; Sagurthi, S. R.; Qureshi, I. A. Leishmania donovani PP2C: Kinetics, structural attributes and in vitro immune response. *Mol. Biochem. Parasitol.* **2018**, *223*, 37−49.

(31) Banerjee, B.; Banerjee, R. Urea unfolding study of E. coli alanyl-tRNA synthetase and its monomeric variants proves the role of c-terminal domain in stability. *J. Amino Acids* **2015**, *2015*, 805681.

(32) Panigrahi, G. C.; Qureshi, R.; Jakkula, P.; Kumar, K. A.; Khan, N.; Qureshi, I. A. Leishmanial aspartyl-tRNA synthetase: Biochemical, biophysical and structural insights. *Int. J. Biol. Macromol.* **2020**, *165*, 2869.

(33) Malavasic, M.; Poklar, N.; Macek, P.; Vesnaver, G. Fluorescence studies of the effect of pH, guanidine hydrochloride and urea on equinatoxin II conformation. *Biochim. Biophys. Acta* **1996**, *1280*, 65−72.

(34) Are, S.; Gatreddi, S.; Jakkula, P.; Qureshi, I. A. Structural attributes and substrate specificity of pyridoxal kinase from Leishmania donovani. *Int. J. Biol. Macromol.* **2020**, *152*, 812−827.

(35) Jakkula, P.; Narsimulu, B.; Qureshi, I. A. Biochemical and structural insights into 6-phosphogluconate dehydrogenase from Leishmania donovani. *Appl. Microbiol. Biotechnol.* **2021**, *105*, 5471−5489.

(36) Myers, J. K.; Pace, C. N.; Scholtz, J. M. Denaturant m values and heat capacity changes: Relation to changes in accessible surface areas of protein unfolding. *Protein Sci.* **1995**, *4*, 2138−2148.

(37) Gonzalez, S. N.; Mills, J. J.; Maugeri, D.; Olaya, C.; Laguera, B. L.; Enders, J. R.; Sherman, J.; Rodriguez, A.; Pierce, J. G.; Cazzulo, J. J.; D'Antonio, E. L. Design, synthesis, and evaluation of substrate - analogue inhibitors of Trypanosoma cruzi ribose 5-phosphate isomerase type B. *Bioorg. Med. Chem. Lett.* **2021**, *32*, 127723.

(38) Webb, B.; Sali, A. Comparative Protein Structure Modeling Using MODELLER. *Curr. Protoc. Bioinf.* **2016**, *54*, 5.6.1−5.6.37.

(39) Laskowski, R. A.; MacArthur, M. W.; Moss, D. S.; Thornton, J. M. PROCHECK: a program to check the stereochemical quality of protein structures. *J. Appl. Crystallogr.* **1993**, *26*, 283−291.

(40) Van Der Spoel, D.; Lindahl, E.; Hess, B.; Groenhof, G.; Mark, A. E.; Berendsen, H. J. C. GROMACS: Fast, flexible, and free. *J. Comput. Chem.* **2005**, *26*, 1701−1718.

(41) Colovos, C.; Yeates, T. O. Verification of protein structures: patterns of nonbonded atomic interactions. *Protein Sci.* **1993**, *2*, 1511−1519.

(42) Lüthy, R.; Bowie, J. U.; Eisenberg, D. Assessment of protein models with three-dimensional profiles. *Nature* **1992**, *356*, 83−85.

(43) Grosdidier, A.; Zoete, V.; Michielin, O. SwissDock, a protein-small molecule docking web service based on EADock DSS. *Nucleic Acids Res.* **2011**, *39*, W270−W277.

(44) Bhat, S. Y.; Qureshi, I. A. Structural and functional basis of potent inhibition of leishmanial leucine aminopeptidase by peptidomimetics. *ACS Omega* **2021**, *6*, 19076−19085.